Theory of anisotropy of two-photon absorption in zinc-blende semiconductors

D. C. Hutchings
Department of Electronics and Electrical Engineering, University of Glasgow, Glasgow G12 8QQ, United Kingdom

B. S. Wherrett
Department of Physics, Heriot-Watt University, Edinburgh EH14 4AS, United Kingdom
(Received 27 September 1993)

The influence of the higher Γ_{15}^{c} conduction-band set on the strength of the two-photon-absorption coefficient, the two-photon linear/circular dichroism, and the two-photon-absorption anisotropy is calculated across the spectral region below the fundamental absorption edge, for the cubic materials GaAs and InSb. The anisotropy is entirely due to the higher band and is predicted to produce up to a 70% variation in the two-photon-absorption coefficient of GaAs as the relative orientation of the optical polarization to the crystal axes is altered. This is in good agreement with recent experiments.

I. INTRODUCTION

The role of two-photon absorption (TPA) in semiconductors is of increasing importance as semiconductor components become employed as nonlinear elements in optical communication and information processing systems. For example, two-photon absorption provides a fundamental limitation for all-optical switching in the transparent spectral region of semiconductors.[1] It has also been recently recognized that ultrafast nonlinear refraction can be related to two-photon absorption through a nonlinear Kramers-Krönig relation.[2,3] Two-photon absorption also has potential applications as a nonlinear spectroscopic technique, providing complementary material information to one-photon-absorption measurements.

For cubic materials (such as zinc-blende semiconductors) the only nonzero components of the first-order optical susceptibility tensor are the equal, diagonal components. Hence, the one-photon-absorption spectrum shows no polarization dependence (and, equally, there is no birefringence). However, the third-order susceptibility tensor contains off-diagonal elements, as a consequence of which the TPA exhibits optical polarization dependence. In the isotropic limit the dependence is manifested by a difference between the TPA coefficients for linear and circular polarized light in single-beam experiments.[4] For two-beam experiments the relative polarization orientation of the beams influences the TPA;[5] this is seen in nondegenerate TPA, for example. Cubic materials have three equivalent orthogonal axes but are not isotropic. Hence, even in single-beam linearly polarized cases, the TPA coefficient should depend on the orientation of the polarization to the crystal axes. It is this orientation dependence that is of major interest in this paper.

Most studies of two-photon absorption in zinc-blende semiconductors have been for a single, plane-polarized beam. The more successful of the theoretical predictions for this case (compared to reliable experimental data) are based on a second-order perturbative method, using the isotropic band-structure model of Kane[6] consisting of the uppermost valence-band set (heavy-hole, light-hole, and sometimes the spin-orbit split-off states) and a single conduction band.[5,7–10] However, as this band-structure model is isotropic (i.e., the band energies depend only on the modulus of the electronic wave vector and not on its direction), it does not provide any orientational dependence. One method of introducing the effects of anisotropy into the band-structure model is to use the band-decoupling scheme of Luttinger and Kohn[11] which provides an anisotropic mixing of the valence bands to order k^2. Dykman and Rubo[12] have used the valence state mixing so obtained to calculate a two-photon anisotropy for GaAs and InSb. However, the conduction-band anisotropy and the effective-mass anisotropies were not included in the above calculation. An alternative approach is to include higher conduction bands in the calculation; the resulting state mixing (e.g., due to the $\mathbf{k}\cdot\mathbf{p}$ perturbation) provides the anisotropic band structure. This approach was considered briefly, for the parabolic-band limit, by Arifzhanov and Ivchenko,[13] who estimated the two-photon anisotropy for Ge. It is well known that the effect of higher bands is also necessary in order to predict correctly the effective-mass values in direct-gap semiconductors.[14,15] In this paper higher conduction bands are considered explicitly and the resulting anisotropies, both of the nonparabolic energy surfaces (the effective masses) and of the state wave functions, are accounted for.

An early experimental investigation of TPA anisotropy was that of Bepko,[16] who measured the crystal orientation dependence of the nonlinear absorption. However, the measurements were obtained with nanosecond pulses and, like many of the earlier measurements of TPA, were dominated by free-carrier absorption of two-photon photogenerated carriers. Van der Ziel[17] obtained an accurate estimate of TPA anisotropy by measuring the band-edge luminescence associated with TPA excitation; the luminescence is insensitive to free-carrier absorption. However, to obtain accurate magnitudes for the TPA coefficients, shorter laser pulsewidths (in picoseconds) must be employed. The TPA anisotropy of GaAs and CdTe has been investigated in such a manner using a

pump-probe technique[18] (which determines all the nonzero $\mathrm{Im}\chi^{(3)}$ tensor elements). Picosecond z scans of a suitably cut crystal of GaAs have also been used.[19]

II. THEORY

For the zinc-blende structure (cubic symmetry class $\bar{4}3m$), out of the 81 third-order susceptibility tensor elements, 21 are nonzero and only 4 of these are independent,[20] $\chi^{(3)}_{xxxx}$, $\chi^{(3)}_{xyxy}$, $\chi^{(3)}_{xyyx}$ and $\chi^{(3)}_{xxyy}$. Furthermore, by restricting the discussion to the degenerate regime (where only one optical frequency is present), intrinsic permutation symmetry reduces the number of independent elements to 3 because

$$\chi^{(3)}_{xyyx}(-\omega,\omega,\omega)=\chi^{(3)}_{xyxy}(-\omega,\omega,\omega)\ . \tag{1}$$

The two-photon-absorption coefficient is directly related to the imaginary part of the third-order susceptibility. For the symmetry appropriate to zinc-blende semiconductors, this relation can be expressed as[18]

$$\beta(\omega)=\frac{3}{2}\frac{\omega}{\varepsilon_0 n_0^2 c^2}[\chi''_{xxxx}\Sigma+2\chi''_{xyxy}(1-\Sigma)+\chi''_{xxyy}(|\hat{\mathbf{e}}\cdot\hat{\mathbf{e}}|^2-\Sigma)]\ , \tag{2}$$

with $\Sigma=\sum_r |e_r|^4$.

Here c is the speed of light in vacuum, ε_0 the permittivity of free space, and n_0 the linear refractive index. The radiation polarization is described by the unit vector $\hat{\mathbf{e}}$, having direction cosines e_r with respect to the three crystalline axes (x,y,z). χ''_{xyxy} is used as a shorthand notation to represent $\mathrm{Im}\chi^{(3)}_{xyxy}(-\omega,\omega,\omega)$, etc. There is a factor-of-3 difference in Eq. (2) with respect to the formula quoted in Ref. 18; this factor is accommodated in the definition of χ_{ijkl} used below.

The calculation of the three, independent tensor elements in the β expression is presented below and in Sec. III. the resulting anisotropy of β, expressed through the Σ factors, and the linear-circular dichroism, expressed through $|\hat{\mathbf{e}}\cdot\hat{\mathbf{e}}|$ and the Σ factors, is discussed in Sec. IV.

From a density-matrix treatment, the third-order susceptibility can, in general, be calculated from[20]

$$\chi^{(3)}_{ijkl}(\omega_1,\omega_2,\omega_3)=-\frac{e^4}{3!\hbar^3\varepsilon_0 m_0^4}\frac{1}{(\omega_1+\omega_2+\omega_3)\omega_1\omega_2\omega_3}\mathbf{S}_T\sum_{g,\alpha,\beta,\gamma}\frac{(\hat{\mathbf{e}}_i^*\cdot\mathbf{p}_{g\alpha})(\hat{\mathbf{e}}_j\cdot\mathbf{p}_{\alpha\beta})(\hat{\mathbf{e}}_k\cdot\mathbf{p}_{\beta\gamma})(\hat{\mathbf{e}}_l\cdot\mathbf{p}_{\gamma g})}{(\Omega_{\alpha g}-\omega_1-\omega_2-\omega_3)(\Omega_{\beta g}-\omega_2-\omega_3)(\Omega_{\gamma g}-\omega_3)}\ , \tag{3}$$

where m_0 is the free-electron mass, $\hat{\mathbf{e}}_i$ is the unit vector in the direction of the *ith* polarization, and $\mathbf{p}_{\alpha\beta}$ and $\hbar\Omega_{\alpha\beta}$ are the momentum matrix element and energy difference, respectively, taken between the states α and β. Here, $\mathbf{S}_T$ denotes that the expression which follows it is to be summed over all permutations which, in the case of the third-order susceptibility, are the 24 permutations of the pairs $(i,-\omega_1-\omega_2-\omega_3)$, (j,ω_1), (k,ω_2), and (l,ω_3). A useful method for generating these is the diagrammatic technique of Ward.[21] Ideally the sum should be performed over all electron states α,β,γ and over all occupied electron states g. In practice, these summations are taken over a limited number of states which are deemed to be dominant.

Two-photon absorption is a resonant effect that occurs in semiconductors when the sum of the two photon energies is equal to the energy difference between a valence band (occupied) and a conduction band (unoccupied). Thus the permutations of Eq. (3) that correspond to two-photon absorption are those four in which the state β is a conduction-band state and (in the degenerate case) $\omega_2=\omega_3=\omega$, $\omega_1=-\omega$. A damping term Γ should be included in the resonant denominator; Γ can be taken to be vanishingly small, allowing the substitution

$$\frac{1}{\Omega_{cv}-2\omega}\rightarrow\frac{1}{\Omega_{cv}-2\omega-i\Gamma}=\frac{1}{\Omega_{cv}-2\omega}+i\pi\delta(\Omega_{cv}-2\omega)\ . \tag{4}$$

Two-photon absorption is manifested by the imaginary δ-function term in Eq. (4), while the real part gives rise to an associated nonlinear refraction.[3] On evaluating Eq. (3) for the three independent two-photon-absorption terms, some simplification is possible by factorizing the terms to give

$$\chi''_{xxxx}=\frac{2\pi e^4}{3\varepsilon_0\hbar^3 m_0^4\omega^4}\sum_{v,c}\left|\sum_i\frac{(\hat{\mathbf{x}}\cdot\mathbf{p}_{iv})(\hat{\mathbf{x}}\cdot\mathbf{p}_{ci})}{\Omega_{iv}-\omega}\right|^2\delta(\Omega_{cv}-2\omega)\ ,$$

$$\chi''_{xyxy}=\frac{2\pi e^4}{3\varepsilon_0\hbar^3 m_0^4\omega^4}\sum_{v,c}\left|\sum_i\frac{(\hat{\mathbf{x}}\cdot\mathbf{p}_{iv})(\hat{\mathbf{y}}\cdot\mathbf{p}_{ci})+(\hat{\mathbf{y}}\cdot\mathbf{p}_{iv})(\hat{\mathbf{x}}\cdot\mathbf{p}_{ci})}{2(\Omega_{iv}-\omega)}\right|^2\delta(\Omega_{cv}-2\omega)\ , \tag{5}$$

$$\chi''_{xxyy}=\frac{2\pi e^4}{3\varepsilon_0\hbar^3 m_0^4\omega^4}\sum_{v,c}\left[\sum_i\frac{(\hat{\mathbf{x}}\cdot\mathbf{p}_{iv})(\hat{\mathbf{x}}\cdot\mathbf{p}_{ci})}{\Omega_{iv}-\omega}\right]^*\left[\sum_j\frac{(\hat{\mathbf{y}}\cdot\mathbf{p}_{jv})(\hat{\mathbf{y}}\cdot\mathbf{p}_{cj})}{\Omega_{jv}-\omega}\right]\delta(\Omega_{cv}-2\omega)\ .$$

Here, the summations are to be performed over conduction-band states c (empty), valence-band states v (filled), and all states i (empty or filled). These will, in general, involve a summation over bands and an integration over k space. However, as the photon momentum is negligible compared to the electronic momentum, only electron states with the same wave vector are coupled and only one integration over k space is required. The first two imaginary susceptibilities χ''_{xxxx} and χ''_{xyxy} can also be derived by a transition-rate approach.[5] The susceptibility term χ''_{xxyy} cannot be obtained directly from a transition-rate approach although the form in which it has been expressed in Eq. (5) is somewhat similar to that of the other tensor elements. It should be noted that the χ''_{xxyy} tensor element does not correspond to an observable two-photon-absorption process, always occurring in combination with at least one of χ''_{xxxx} or χ''_{xyxy} in appropriate TPA coefficients.

The band structure used in the calculations in this paper is that employed by Pfeffer and Zawadzki,[14] consisting of a triplet valence-band set, a single conduction-band set, and the next-higher conduction-band set (triplet), as shown schematically in Fig. 1. At zone center ($k=0$), the basis wave functions for the singlet states S have the symmetry of s-like atomic wave functions and the basis wave functions for the valence (conduction) triplet states $X,Y,Z(X',Y',Z')$ have the symmetry of p-like atomic wave functions. The perturbation Hamiltonian which results in a mixing of these states due to $\mathbf{k}\cdot\mathbf{p}$ and spin-orbit interactions is given by

$$H'=\frac{\hbar}{m_0}\mathbf{k}\cdot\mathbf{p}+\frac{\hbar}{4m_0^2c^2}[\nabla V\times\mathbf{p}]\cdot\sigma_p \ , \tag{6}$$

where V is the periodic crystal potential and σ_p is here the Pauli spin matrix. The band-structure calculations are simplified by using the basis functions of Table I rather than X, Y, etc. The $\mathbf{k}=0$ Hamiltonian is almost diagonalized for these functions; the only off-diagonal elements

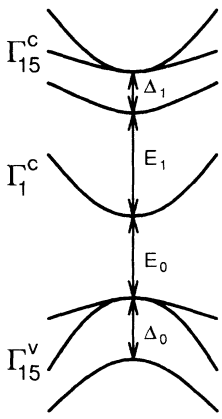

FIG. 1. Schematic of the model used for the semiconductor band structure in the vicinity of the Γ point of the Brillouin zone, consisting of the highest valence-band set Γ_{15}^v and the two lowest conduction-band sets, Γ_1^c and Γ_{15}^c. The degeneracy of the Γ_{15} triplet states at $k=0$ is lifted by the spin-orbit interaction.

TABLE I. Basis Bloch electronic wave functions. Here the shorthand notation $R_\pm=(X\pm iY)/\sqrt{2}$ is used.

u_1	$\sqrt{\frac{1}{3}}R'_+\downarrow-\sqrt{\frac{2}{3}}Z'\uparrow$	u_8	$\sqrt{\frac{1}{3}}R'_-\uparrow+\sqrt{\frac{2}{3}}Z'\downarrow$
u_2	$-R'_-\downarrow$	u_9	$R'_+\uparrow$
u_3	$\sqrt{\frac{2}{3}}R'_+\downarrow+\sqrt{\frac{1}{3}}Z'\uparrow$	u_{10}	$\sqrt{\frac{2}{3}}R'_+\uparrow/\sqrt{\frac{1}{3}}Z'\downarrow$
u_4	$iS\downarrow$	u_{11}	$iS\uparrow$
u_5	$\sqrt{\frac{1}{3}}R_+\downarrow-\sqrt{\frac{2}{3}}Z\uparrow$	u_{12}	$\sqrt{\frac{1}{3}}R_-\uparrow+\sqrt{\frac{2}{3}}Z\downarrow$
u_6	$-R_-\downarrow$	u_{13}	$R_+\uparrow$
u_7	$\sqrt{\frac{2}{3}}R_+\downarrow+\sqrt{\frac{1}{3}}Z\uparrow$	u_{14}	$\sqrt{\frac{2}{3}}R_+\uparrow/\sqrt{\frac{1}{3}}Z\downarrow$

involve the relatively small parameter $\bar{\Delta}$, which is due to the spin-orbit interaction between the valence and higher-conduction bands. The resulting Hamiltonian at finite $\mathbf{k}$ is given in Table II, in which the spin-orbit and momentum matrix element parameters are defined by

$$P_0=\langle S|H_1|X\rangle \ , \quad P_1=\langle S|H_1|X'\rangle \ , \quad Q=\langle Z|H_1|Y'\rangle \ , \tag{7a}$$

$$\Delta_0=\langle X|H_2|Y\rangle \ ,$$

$$\Delta_1=-\langle X'|H_2|Y'\rangle \ , \tag{7b}$$

$$\bar{\Delta}=-\langle X|H_2|Y'\rangle \ ,$$

with

$$H_1=\frac{-i\hbar p_x}{m_0} \ , \quad H_2=\frac{3i\hbar}{4m_0^2c^2}\left[\frac{\partial V}{\partial x}p_y-\frac{\partial V}{\partial y}p_x\right] . \tag{7c}$$

If $\bar{\Delta}$ were zero, then the diagonal terms of the Hamiltonian matrix would be the zero-$\mathbf{k}$ energy levels.

The 14×14 matrix diagonalization was performed numerically and so automatically included the higher-order terms in k that give rise to such effects as nonparabolicity, which are important in two-photon-absorption calculations.[5,8,22] In the determination of the optical susceptibilities, the matrix elements $(e/m_0c)\mathbf{A}\cdot\mathbf{p}$ are required. These may be obtained, within a constant factor, by taking the $\mathbf{k}\cdot\mathbf{p}$ elements of Table II and replacing $\mathbf{k}$ by the polarization unit vector $\mathbf{e}$.

III. NUMERICAL RESULTS

The band-structure parameters used in the present calculations are given in Table III. These are the values obtained by fitting data for low-temperature GaAs (Ref. 14) and InSb (Ref. 15). Figure 2 demonstrates the resulting anisotropy of the GaAs energy levels. The valence and conduction levels are plotted for $\mathbf{k}$ values in the [001] and [011] directions. It can be seen that the dependence on $|\mathbf{k}|$ is slightly different for the two directions (most obviously for the heavy-hole band) and it is noticeable that the anisotropy gives rise to a spin splitting in the band energies for $\mathbf{k}$ parallel to the [011] direction.

Figure 3 shows the result of the calculation for the two-photon-absorption susceptibilities for GaAs using Eq. (5); Fig. 3(a) corresponds to the 14-band model discussed above, while, for comparison, Fig. 3(b) corresponds to the simpler isotropic band-structure model with the same band parameters but where the upper Γ_{15}^c

TABLE II. Hamiltonian matrix including $\mathbf{k}\cdot\mathbf{p}$ and spin-orbit interactions using the basis set given in Table I is given by $\mathbf{H}'+(C+1)(\hbar^2k^2/2m_0^2)\mathbf{I}$ where the second term describes the isotropic free-mass and distant band contributions and $\mathbf{H}'$ is given in the following table (from Ref. 14). As this matrix is Hermitian, only the upper triangle is shown. The shorthand notation $k_\pm=(k_x\pm ik_y)/\sqrt{2}$ is employed. Due to the appearance of the off-diagonal spin-orbit term $\bar{\Delta}$, the diagonal terms are not the observable energies at $k=0$, but are modified, $G_{v1}=(E_1+\Delta_1+E_0)/2-[(E_1+\Delta_1+E_0)^2/4-\bar{\Delta}^2/9]^{1/2}$, $G_{v2}=(E_1+E_0-\Delta_0)/2-[(E_1+E_0+\Delta_0)^2/4-4\bar{\Delta}^2/9]^{1/2}$, $G_{c3}=(E_1+\Delta_1+E_0)/2+[(E_1+\Delta_1+E_0)^2/4-\bar{\Delta}^2/9]^{1/2}$, $G_{c2}=(E_1+E_0-\Delta_0)/2+[(E_1+E_0+\Delta_0)^2/4-4\bar{\Delta}^2/9]^{1/2}$, and $G_{c1}=E_0$.

G_{c3}	0	0	$\sqrt{\frac{1}{3}}P_1k_-$	$\frac{1}{3}\bar{\Delta}$	$\sqrt{\frac{1}{3}}Qk_z$	0	0	0	0	$-\frac{\sqrt{2}}{3}P_1k_z$	0	$-\sqrt{\frac{2}{3}}Qk_-$	Qk_+
	G_{c3}	0	$-P_1k_+$	$-\sqrt{\frac{1}{3}}Qk_z$	$\frac{1}{3}\bar{\Delta}$	$-\sqrt{\frac{2}{3}}Qk_z$	0	0	0	0	$-\sqrt{\frac{2}{3}}Qk_-$	0	$\sqrt{\frac{1}{3}}Qk_-$
		G_{c2}	$\sqrt{\frac{2}{3}}P_1k_-$	0	$\sqrt{\frac{2}{3}}Qk_z$	$-\frac{2}{3}\bar{\Delta}$	0	0	0	$\sqrt{\frac{1}{3}}P_1k_z$	$-Qk_+$	$\sqrt{\frac{1}{3}}Qk_-$	0
			G_{c1}	$\sqrt{\frac{1}{3}}P_0k_+$	$-P_0k_-$	$\sqrt{\frac{2}{3}}P_0k_+$	$\sqrt{\frac{2}{3}}P_1k_z$	0	$-\sqrt{\frac{1}{3}}P_1k_z$	0	$\sqrt{\frac{2}{3}}P_0k_z$	0	$-\sqrt{\frac{1}{3}}P_0k_z$
				G_{v1}	0	0	0	$\sqrt{\frac{2}{3}}Qk_-$	$-Qk_+$	$-\sqrt{\frac{2}{3}}P_0k_z$	0	0	0
					G_{v1}	0	$\sqrt{\frac{2}{3}}Qk_-$	0	$-\sqrt{\frac{1}{3}}Qk_-$	0	0	0	0
						G_{v2}	Qk_+	$-\sqrt{\frac{1}{3}}Qk_-$	0	$\sqrt{\frac{1}{3}}P_0k_z$	0	0	0
							G_{c3}	0	0	$\sqrt{\frac{1}{3}}P_1k_+$	$\frac{1}{3}\bar{\Delta}$	$\sqrt{\frac{1}{3}}Qk_z$	0
								G_{c3}	0	P_1k_-	$-\sqrt{\frac{1}{3}}Qk_z$	$\frac{1}{3}\bar{\Delta}$	$-\sqrt{\frac{2}{3}}Qk_z$
									G_{c2}	$\sqrt{\frac{2}{3}}P_1k_+$	0	$\sqrt{\frac{2}{3}}Qk_z$	$-\frac{2}{3}\bar{\Delta}$
										G_{c1}	$\sqrt{\frac{1}{3}}P_0k_-$	P_0k_+	$\sqrt{\frac{2}{3}}P_0k_-$
											G_{v1}	0	0
												G_{v1}	0
													G_{v2}

conduction-band set is neglected.[6,4] In each case the three individual tensor elements χ''_{xxxx}, χ''_{xyxy}, and χ''_{xxyy} are shown. It can be seen that the effect of the upper conduction-band set is to reduce χ''_{xxxx} slightly (by around 15% at its peak) but to enhance significantly the two off-diagonal tensor elements χ''_{xyxy} and χ''_{xxyy}. In particular, χ''_{xxyy} has increased by more than a factor of 2 for frequencies close to the one-photon-absorption edge. It has previously been noted that this tensor element is particularly sensitive to the details of the band-structure model with respect to the inclusion of the valence split-off band,[4] so it is not too surprising that the same is true for the inclusion of the upper conduction-band set.

Figure 4 shows the individual contributions to the $\mathrm{Im}\chi^{(3)}$ tensor elements from each of the valence-band to conduction-band transitions. Qualitatively, these results are similar to those obtained without the inclusion of the upper conduction-band set.[4] Note the relative contributions from the heavy-hole and light-hole valence bands for each of the tensor elements just above the two-photon band edge. For χ''_{xxxx}, the light-hole term is larger than the heavy-hole term; for χ''_{xyxy}, the heavy-hole term is larger than the light-hole term; and for χ''_{xxyy}, the heavy-hole term is negative. It should be noted that χ''_{xxyy} does

TABLE III. Data for the two semiconductors studied in this paper obtained by low-temperature magneto-optical measurements (Refs. 14 and 15). The momentum parameters are defined $E_{P0}=2m_0P_0^2/\hbar^2$, etc. All values are in electron volts.

	GaAs	InSb
E_0	1.519	0.2352
E_1	2.969	3.11
Δ_0	0.341	0.803
Δ_1	0.171	0.39
$\bar{\Delta}$	−0.061	−0.163
E_{P0}	27.86	23.43
E_{P1}	2.36	4.923
E_Q	15.56	13.99

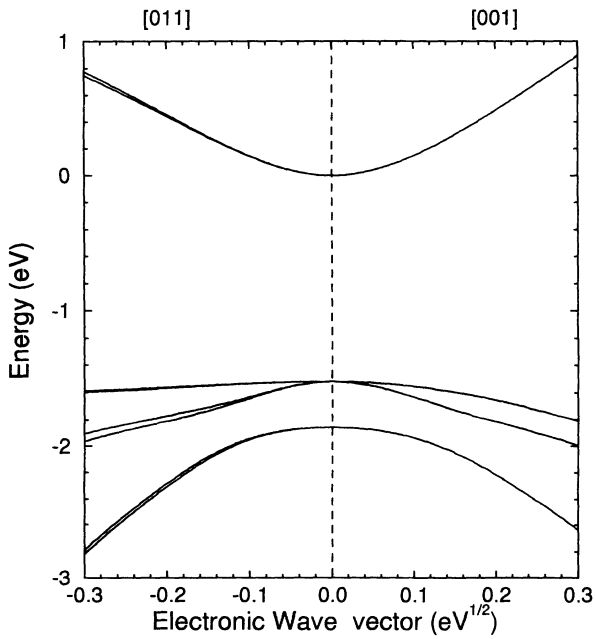

FIG. 2. Calculated band structure near the Γ point of the Brillouin zone for two different directions in k space, $\mathbf{k}\|[001]$ and $\mathbf{k}\|[011]$. The electronic wave vector $\mathbf{k}$ has been scaled by $\hbar/\sqrt{2m_0}$ to give a value in $(\mathrm{eV})^{1/2}$. It can be seen that the band structure is anisotropic and for the [011] direction the spin degeneracy is lifted.

not correspond to a real transition, i.e., the negative value does not correspond to two-photon gain without inversion. This negative value results in a partial cancellation with the light-hole term, although not to the same degree as in the calculation without the upper band set. The threshold of the split-off terms occurs at $(E_0+\Delta_0)/2$ and results in obvious gradient changes in the total $\mathrm{Im}\chi^{(3)}$ tensor elements. It is interesting to note that the split-off term is large for χ''_{xxyy} but insignificant for χ''_{xyxy}.

Figure 5 shows the same three tensor elements as a function of frequency, for the narrow-gap semiconductor InSb. For comparison the dashed lines show the same quantities calculated without the influence of the upper conduction-band set. In this case the upper conduction bands provide a very much smaller perturbation in comparison to GaAs. This is to be expected as the upper conduction bands (and split-off valence band) are relatively far away in energy terms.

The effect of the upper conduction-band levels is threefold. First, the mixing of the upper conduction states with the lower conduction and valence bands perturbs the energies leading to anisotropic bands and spin splitting. Second, the upper conduction-band wave functions

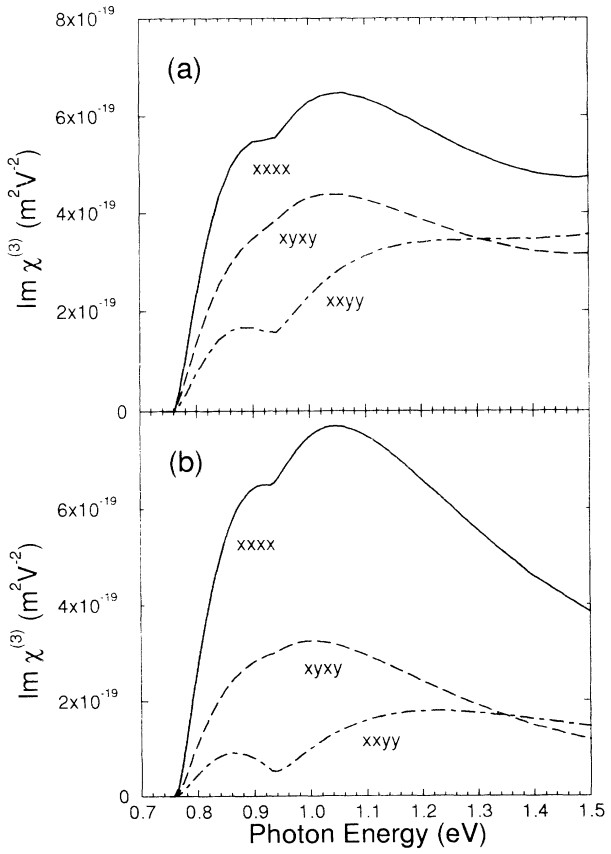

FIG. 3. The three independent, degenerate $\mathrm{Im}\chi^{(3)}$ tensor elements calculated as a function of photon energy in the range $0.5<\hbar\omega/E_0<1$ for GaAs based on low-temperature band-structure data. (a) shows the anisotropic result obtained by including the upper conduction-band set Γ_{15}^c and (b) shows the isotropic result obtained without the inclusion of the upper conduction-band set.

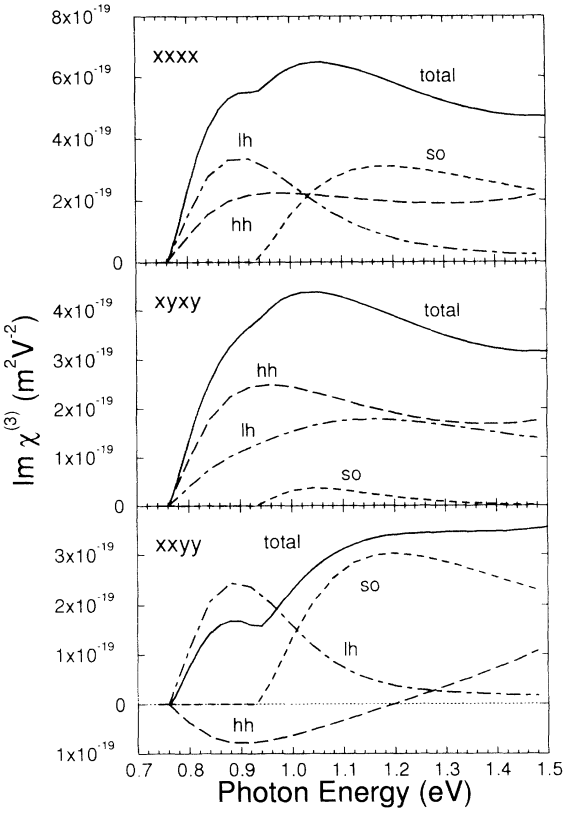

FIG. 4. Individual contributions to the $\mathrm{Im}\chi^{(3)}$ tensor elements for GaAs resulting from contributions between the various valence bands, as indicated, and the conduction band, plotted as a function of photon energy. The total contribution to each tensor element is simply the sum of the individual band contributions shown.

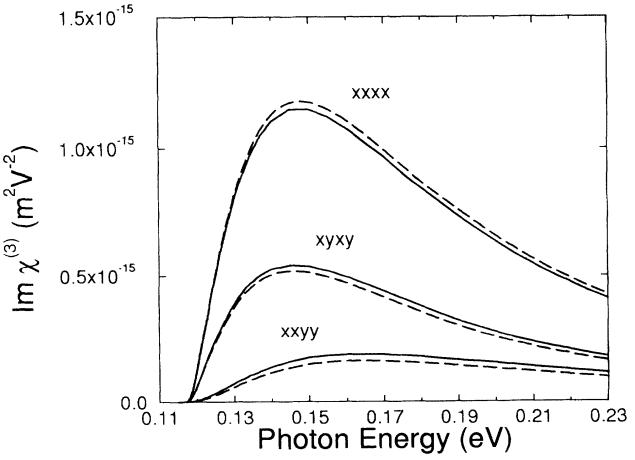

FIG. 5. The three independent, degenerate $\mathrm{Im}\chi^{(3)}$ tensor elements calculated as a function of photon energy in the range $0.5<\hbar\omega/E_0<1$ for InSb, based on low-temperature band-structure data. The solid lines show the anisotropic result obtained by including the upper conduction-band set Γ_{15}^c and the dashed lines show the isotropic result obtained when this band set is neglected.

X', Y', Z' mix with the lower states and so modify the optical coupling between the lower states. Third, the upper conduction-band states appear as additional intermediate levels in two-photon absorption.

For higher-band intermediate levels the TPA transitions are known as allowed-allowed and a TPA coefficient proportional to the valence-conduction joint density of states, $(\hbar\omega - E_0/2)^{1/2}$, is expected. At finite $\mathbf{k}$, however, the mixed parity of the states produces self-transitions and the valence- or conduction-band levels themselves can act as intermediate states. The resulting allowed-forbidden TPA coefficient is proportional to $(\hbar\omega - E_0/2)^{3/2}$. The allowed-allowed scheme must dominate at frequencies sufficiently close to the two-photon band edge, although further complications due to Coulombic-excitation effects are also important in this region. The allowed-forbidden terms are known to dominate away from the edge. This is brought out clearly in Fig. 6, which shows the susceptibility tensor elements for GaAs in Fig. 3(a), but now plotted as a function of $(\hbar\omega - E_0/2)$ on a log-log plot in a manner similar to that of Ref. 17. The gradients of the curves in Fig. 6 are equal to $\frac{1}{2}$ only for a regime extremely close to the edge (within 10^{-5} eV for the case of χ_{xxxx}). The gradient is $\frac{3}{2}$ for intermediate photon energies, and deviates from this at the highest energies. Allowed-forbidden transitions still dominate in the latter regime but the ω^{-4} factor [in Eq. (5)] reduces the dispersion. It can also be seen from Fig. 6 that the allowed-allowed contribution for χ''_{xyxy} is very much larger than the other two tensor elements (about a factor of 60 greater than χ''_{xxxx}). This is because the optical matrix element Q connects two electron p-like states which are mutually orthogonal both to each other and to the optical polarization, but the optical matrix element P_1 (and P_0) connects a p-like state parallel to the optical polarization to an s-like state [Eq. (7a)]. Therefore, the result is much greater when the two optical polarization vectors in the $\chi^{(3)}$ calculation are mutually orthogonal. The implication is that for circularly polarized light the allowed-allowed mechanism remains dominant for higher energies, although still only to 1 meV above the edge; it is still very doubtful whether the square-root frequency dependence could be observed experimentally.

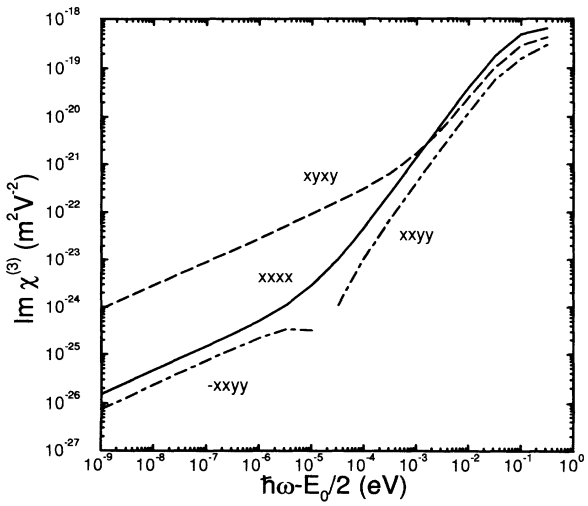

FIG. 6. Calculated behavior of the $\mathrm{Im}\chi^{(3)}$ tensor elements close to the two-photon band edge plotted on a log-log plot as a function of the difference between the photon energy and half the fundamental band gap.

IV. THE TWO-PHOTON-ABSORPTION ANISOTROPY

From a practical viewpoint it is useful to define three independent parameters that describe the strength, anisotropy, and dichroism of the two-photon absorption. First, the obvious choice for the strength is the susceptibility tensor component χ''_{xxxx}. Second, the anisotropy parameter is conventionally defined for TPA as

$$\sigma = \frac{\chi''_{xxxx} - \chi''_{xxyy} - 2\chi''_{xyxy}}{\chi''_{xxxx}} \tag{8}$$

and is zero, from symmetry considerations, in the isotropic limit. Similar ratios can be employed with other third-order nonlinear processes to obtain a measure of the anisotropy—for example, third-harmonic generation.[23,24] Third, for reasons apparent below, we define an incremental TPA dichroism parameter δ as

$$\delta = \frac{\chi''_{xxxx} + \chi''_{xxyy} - 2\chi''_{xyxy}}{2\chi''_{xxxx}} . \tag{9}$$

With these definitions, Eq. (2) can be reexpressed for linearly polarized light as

$$\beta^L(\theta,\phi) = \beta^L[001]\{1 - \sigma[\sin^2(2\theta) + \sin^4(\theta)\sin^2(2\phi)]/2\} , \tag{10}$$

where θ and ϕ are the spherical polar coordinates of $\hat{\mathbf{e}}$, defined with respect to a crystal axis, and $\beta^L[001]$ is the TPA coefficient for radiation linearly polarized along the [001], or equivalent, crystal axis.

For circularly polarized light the corresponding angles θ_κ and ϕ_κ, which define the radiation propagation direction $\hat{\boldsymbol{\kappa}}$, uniquely determine the orientation dependence of the TPA:

$$\beta^c(\theta_\kappa,\phi_\kappa) = \beta^L[001]\{1 - \delta - \sigma[\sin^2(2\theta_\kappa) + \sin^4(\theta_\kappa)\sin^2(2\phi_\kappa)]/8\} . \tag{11}$$

The practical parameters may be measured, for example, for light propagating along one of the crystal axes, by the choice of two linear polarization configurations and one circular polarization:

$$\beta^L[001] = \frac{3}{2}\frac{\omega}{\varepsilon_0 n_0^2 c^2}\chi''_{xxxx} , \tag{12}$$

$$\frac{\beta^L[001] - \beta^L[011]}{\beta^L[001]} = \frac{\sigma}{2} , \tag{13}$$

$$\frac{\beta^L[001] - \beta^C(\theta_\kappa = 0)}{\beta^L[001]} = \delta . \tag{14}$$

This latter result explains our choice of definition for the incremental dichroism parameter δ. The dichroism is not uniquely defined in the anisotropic case, depending on θ and ϕ of the linearly polarized radiation and θ_κ and ϕ_κ of the circularly polarized. For propagation in the [111] direction, β^L shows no angular variation; indeed, the higher bands have almost no influence on the dichroism for this configuration, as shown in Fig. 7.

The influence of the higher Γ_{15}^c band set on the practical TPA parameters can now be determined by comparison with Ref. 4 in which χ''_{xxxx} and δ were evaluated for the valence and conduction-band model, ignoring the higher levels. This latter model is completely isotropic and σ is zero at all frequencies. The effect of the higher bands on the TPA strengths for GaAs and InSb were indicated in Figs. 3 and 5 and discussed in Sec. III. Figure 7(a) shows the calculated frequency dependences of σ, and Figs. 7(b) shows δ calculations for the two models. Note that σ is negative for both GaAs and InSb at all frequencies. Both examples show a sizable dispersion in σ, which increases by approximately a factor of 2 from its value just above the two-photon band edge to that at the one-photon-absorption edge. σ also becomes large and negative close to the two-photon band edge; this can be explained by the presence of allowed-allowed transitions (particularly for the χ''_{xyxy} tensor element), as discussed above. The anisotropy is quite small in the case of InSb, reflecting the fact that the electronic band structure is fairly close to being isotropic.[15] However, in the case of GaAs, the predicted two-photon-absorption anisotropy is substantial.

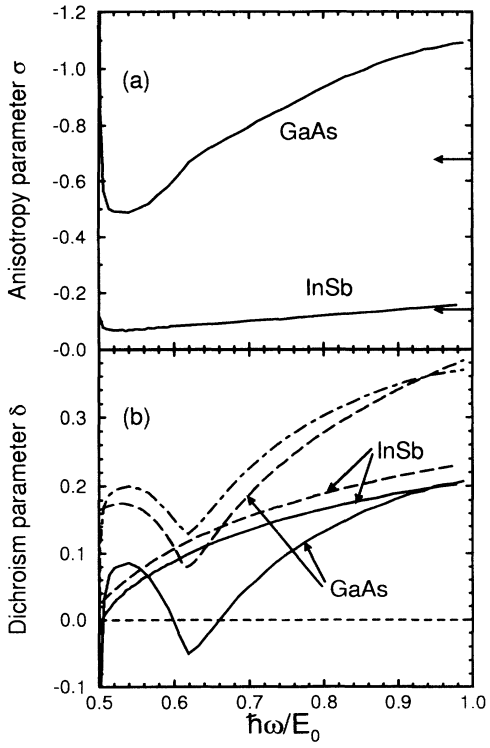

FIG. 7. The two-photon anisotropy parameter σ and the incremental parameter δ [as defined in Eqs. (8) and (9)] plotted as a function of $\hbar\omega/E_0$ for the materials GaAs and InSb. The arrows in (a) indicate σ values obtained from the formula $\sigma=-2E_0(E_0+E_1)^{-1}$. (b) The solid lines are the present calculation and the dashed lines are the results of the isotropic model (ignoring the Γ_{15}^c states). The dot-dashed line corresponds to the incremental dichroism for the anisotropic model for radiation propagation in the [111] crystallographic direction.

van der Ziel used measurements of the band-edge luminescence as a consequence of TPA excitation to determine the TAP anisotropy coefficient in GaAs.[17] A value of $\sigma=-0.45+0.06$ was obtained at a photon energy of 0.8 eV and for low temperature. From Fig. 7(a) the predicted result at this frequency is $\sigma=-0.48$. Dvorak *et al.*[18] have recently measured the value of the two-photon anisotropy parameter in GaAs at room temperature at a wavelength of 950 nm and obtained a value of $\sigma=-0.76$, and DeSalvo *et al.*[19] have obtained a similar value at 1064 nm, $\sigma=-0.74\pm0.18$. The predicted results at the equivalent values of $\hbar\omega/E_0$ are $\sigma\cong-1.0$ for $\lambda=950$ nm and $\sigma\cong-0.9$ at $\lambda=1$ μm, although it should be noted that this calculation is based on band-structure data obtained at low temperatures, whereas the experimental values correspond to room temperature. The equivalent value for σ at 1 μm from the calculations of Dykman and Rubo[12] (low-temperature band-structure data), which include only the effects of valence-band mixing, is $\sigma=-0.4$. Arifzhanov and Ivchenko[13] estimate the anisotropy parameter to be proportional to $E_Q E_0 E_{P0}^{-1} E_1^{-1}$; this provides a simple explanation of the difference in magnitude between GaAs and InSb but the positive sign is in contradiction with the results above. The first-estimate expression $\sigma=-2E_0(E_0+E_1)^{-1}$, given in Ref. 17, does, however, prove to be a very sensible measure of the anisotropy, as indicated by the arrows in Fig. 7.

To illustrate more clearly the effects of anisotropy on the TPA coefficient, the angular variations of β^L and β^C are shown in Figs. 8(a) and 8(b) for the GaAs (950 nm) case for which $\sigma=-1.0$, $\delta=0.18$. the maximum variation in the linear-polarization coefficient is

$$\beta^L[111]/\beta^L[001]=(1-2\sigma/3)\cong1.7\ .$$

The spectral dependence of specific coefficients is demonstrated in Fig. 9, for both linear and circular cases. Thus, comparing the coefficients for light propagating along one crystal axis and either circularly polarized, or linearly polarized along another axis, then in the range

$$0.75\text{ eV}<\hbar\omega<1.0\text{ eV}\ ,$$

the dichroism is close to unity. In fact, around the threshold for the split-off-band to conduction-band two-photon transitions, circularly polarized light experiences a larger two-photon-absorption coefficient than linear polarized light. This contrasts with the isotropic model where the linearly polarized light experiences a significantly larger two-photon-absorption coefficient compared to circularly polarized light, at all frequencies below the one-photon-absorption band edge.[4] For propagation in the [011] direction, however the dichroism with respect to light polarized along $[11\bar{1}]$ can be as large as

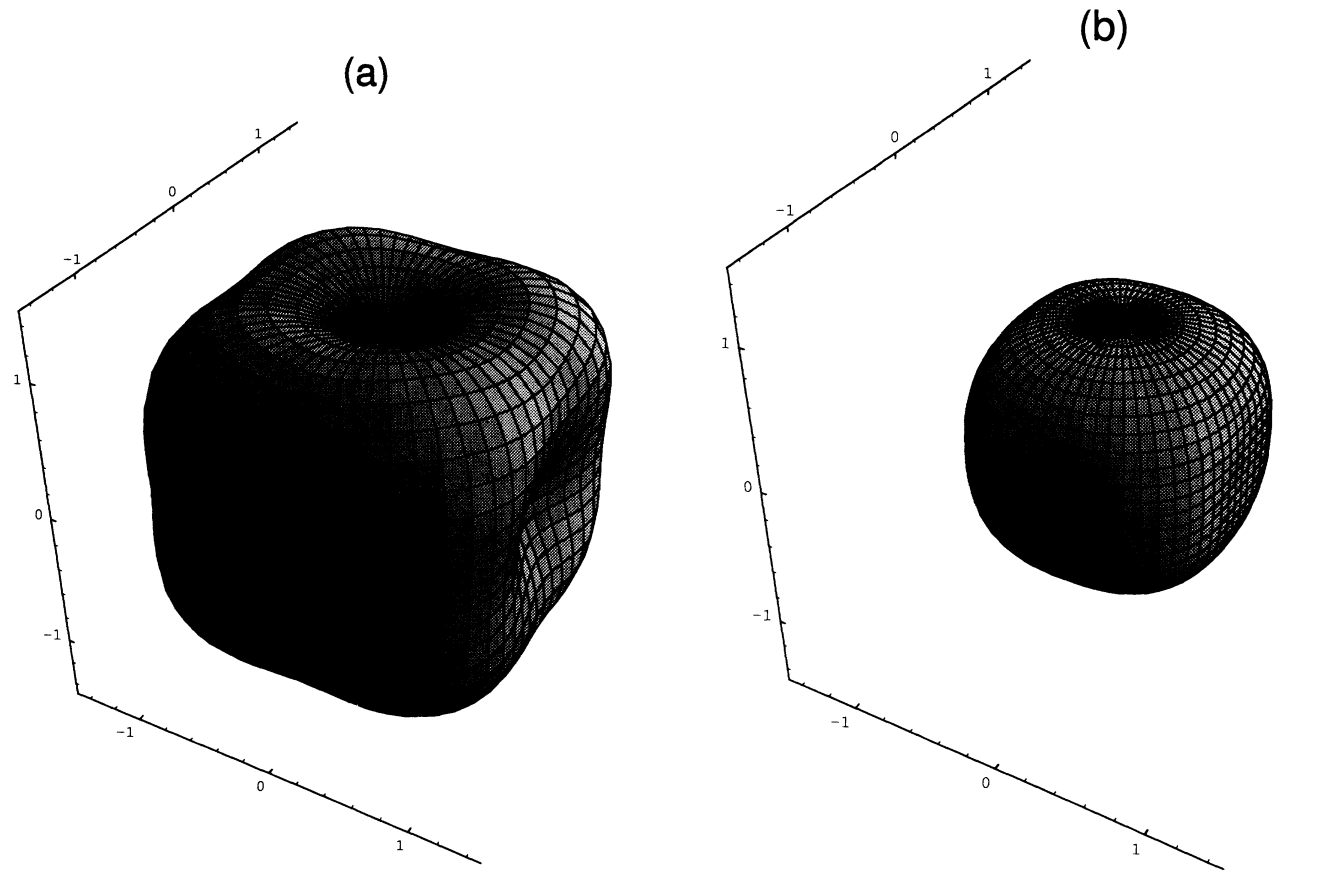

FIG. 8. The anisotropy of the two-photon-absorption coefficients of GaAs calculated from the present model: (a) For linearly polarized light, $\beta^L(\theta,\phi)/\beta^L[001]$ is plotted as a function of angle. The origin for the polarization vector $\hat{\mathbf{e}}$ is at the center of the figure. (b) For circularly polarized light, $\beta^C(\theta_\kappa,\phi_\kappa)/\beta^L[001]$ is plotted as a function of the orientation of the propagation direction $\hat{\kappa}$. The axes in the figures correspond to the crystallographic-axis directions.

1.8, which exceeds (by 0.3) the maximum dichroism predicted by the isotropic model.

V. CONCLUSION

In this paper the anisotropy of two-photon absorption in the zinc-blende semiconductors GaAs and InSb has been determined using the anisotropic band-structure model obtained with the inclusion of the Γ_{15}^c conduction-band set.[14] The values obtained for the anisotropy parameter σ are in good agreement with recent single-wavelength experiments in GaAs.[17,18] The values are quite substantial and give a two-photon-absorption coefficient at 1 μm for light polarized along the [111] axis that is about 70% larger than that for light polarized along [001]. This confirms the importance of specifying the crystal orientation when reporting two-photon-absorption coefficients. In contrast, the predicted two-photon anisotropy for InSb is small with a predicted variation in the two-photon-absorption coefficient of 10% or less for different linear polarization orientations. This reflects the fact that the band structure of InSb around the Γ point deviates only marginally from the isotropic case. The observed anisotropy in GaAs and CdTe is believed to be dominated by the role of the higher Γ_{15}^c conduction levels in both the energy eigenvalues and eigenfunctions of those valence and conduction levels that are two-photon resonant. The role of the higher band as an intermediate level is significant in only a very small and experimentally probably inaccessible energy range. These allowed-allowed transitions are, however, predicted to produce highly anisotropic two-photon absorption. The success of the formula $\sigma=-2E_0(E_0+E_1)^{-1}$ in

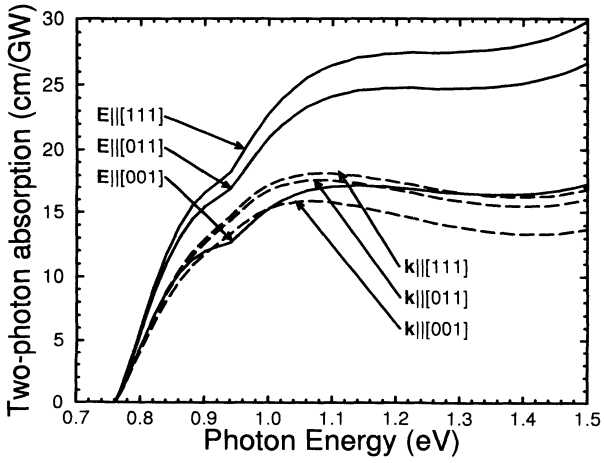

FIG. 9. The spectra of two-photon-absorption coefficients of GaAs, demonstrating both anisotropy and linear-circular dichroism.

determining the approximate values of σ for both GaAs and InSb suggests that for the wide-gap materials (e.g., ZnSe and cubic ZnS), the anisotropy will be larger than that of GaAs, leading to 100% variations in the two-photon coefficients.

The present calculation indicates that there should be a substantial dispersion in the two-photon anisotropy, which increases by around a factor of 2 from just above the two-photon band edge to close to the one-photon band edge. The influence of the higher bands on the strength of the isotropic contribution $\beta^L[001]$ to the (allowed-forbidden) two-photon absorption is shown to be a change of less than 20% for GaAs and 3% for InSb.

The two-photon absorption for circularly polarized light is predicted to be less anisotropic than that for linearly polarized light. An incremental dichroism parameter is defined in terms of the nonlinear susceptibilities, in a manner similar to the anisotropy parameter; the relative TPA coefficients are conveniently expressed in terms of these two parameters. The linear-circular dichroism is predicted to less than 1.3 for GaAs at all relevant frequencies.

ACKNOWLEDGMENTS

D. C. Hutchings gratefully acknowledges support from the Royal Society of Edinburgh, Scottish Office Education Department. The authors also thank W. A. Schroeder and A. L. Smirl of the University of Iowa, E. W. Van Stryland of the University of Central Florida, and C. R. Pidgeon of Heriot-Watt University for stimulating discussions that prompted the present study.

[1]V. Mizrahi, K. W. DeLong, G. I. Stegeman, M. A. Saifi, and M. J. Andrejco, Opt. Lett. **14**, 1140 (1989).
[2]D. C. Hutchings, M. Sheik-Bahae, D. J. Hagan, and E. W. Van Stryland, Opt. Quantum Electron. **24**, 1 (1992).
[3]M. Sheik-Bahae, D. C. Hutchings, D. J. Hagan, and E. W. Van Stryland, IEEE J. Quantum Electron. **27**, 1296 (1991).
[4]D. C. Hutchings and B. S. Wherrett, Opt. Mater. (to be published).
[5]D. C. Hutchings and E. W. Van Stryland, J. Opt. Soc. Am. B **9**, 2065 (1992).
[6]E. O. Kane, J. Phys. Chem. Solids **1**, 249 (1957).
[7]C. C. Lee and H. Y. Fan, Phys. Rev. B **9**, 3502 (1974).
[8]M. H. Weiler, Solid State Commun. **39**, 937 (1981).
[9]E. W. Van Stryland, H. Vanherzeele, M. A. Woodall, M. J. Soileau, A. L. Smirl, S. Guha, and T. F. Boggess, Opt. Eng. **24**, 613 (1985).
[10]B. N. Murdin, C. R. Pidgeon, A. K. Kar, D. A. Jaroszynski, J.-M. Ortega, R. Prazeres, F. Glotin, and D. C. Hutchings, Opt. Mater. **2**, 89 (1993).
[11]J. M. Luttinger and W. Kohn, Phys. Rev. **97**, 869 (1955).
[12]M. I. Dykman and Y. G. Rubo, Phys. Rev. B **45**, 5926 (1992).
[13]S. B. Arifzhanov and E. L. Ivchenko, Fiz. Tverd. Tela (Leningrad) **17**, 81 (1975) [Sov. Phys.—Solid State **17**, 46 (1975)].
[14]P. Pfeffer and W. Zawadzki, Phys. Rev. B **41**, 1561 (1990).
[15]W. Zawadzki, I. T. Yoon, C. L. Littler, X. N. Song, and P. Pfeffer, Phys. Rev. B **46**, 9469 (1992).
[16]S. J. Bepko, Phys. Rev. B **12**, 669 (1975).
[17]J. P. van der Ziel, Phys. Rev. B **16**, 2775 (1977).
[18]M. D. Dvorak, W. A. Schroeder, D. R. Andersen, A. L. Smirl, and B. S. Wherrett, IEEE J. Quantum Electron. (to be published).
[19]R. DeSalvo, M. Sheik-Bahae, A. A. Said, D. J. Hagan, and E. W. Van Stryland, Opt. Lett. **18**, 194 (1993).
[20]P. N. Butcher and D. Cotter, in *The Elements of Nonlinear Optics*, edited by P. L. Knight and W. J. Firth, Cambridge Studies in Modern Optics Vol. 9 (Cambridge University Press, Cambridge, England, 1990).
[21]J. F. Ward, Rev. Mod. Phys. **37**, 1 (1965).
[22]C. R. Pidgeon, B. S. Wherrett, A. M. Johnston, J. Dempsey, and A. Miller, Phys. Rev. Lett. **42**, 1785 (1979).
[23]C. Flytzanis, Phys. Lett. A **31**, 273 (1970).
[24]D. J. Moss, E. Ghahramani, J. E. Sipe, and H. M. van Driel, Phys. Rev. B **41**, 1542 (1990).

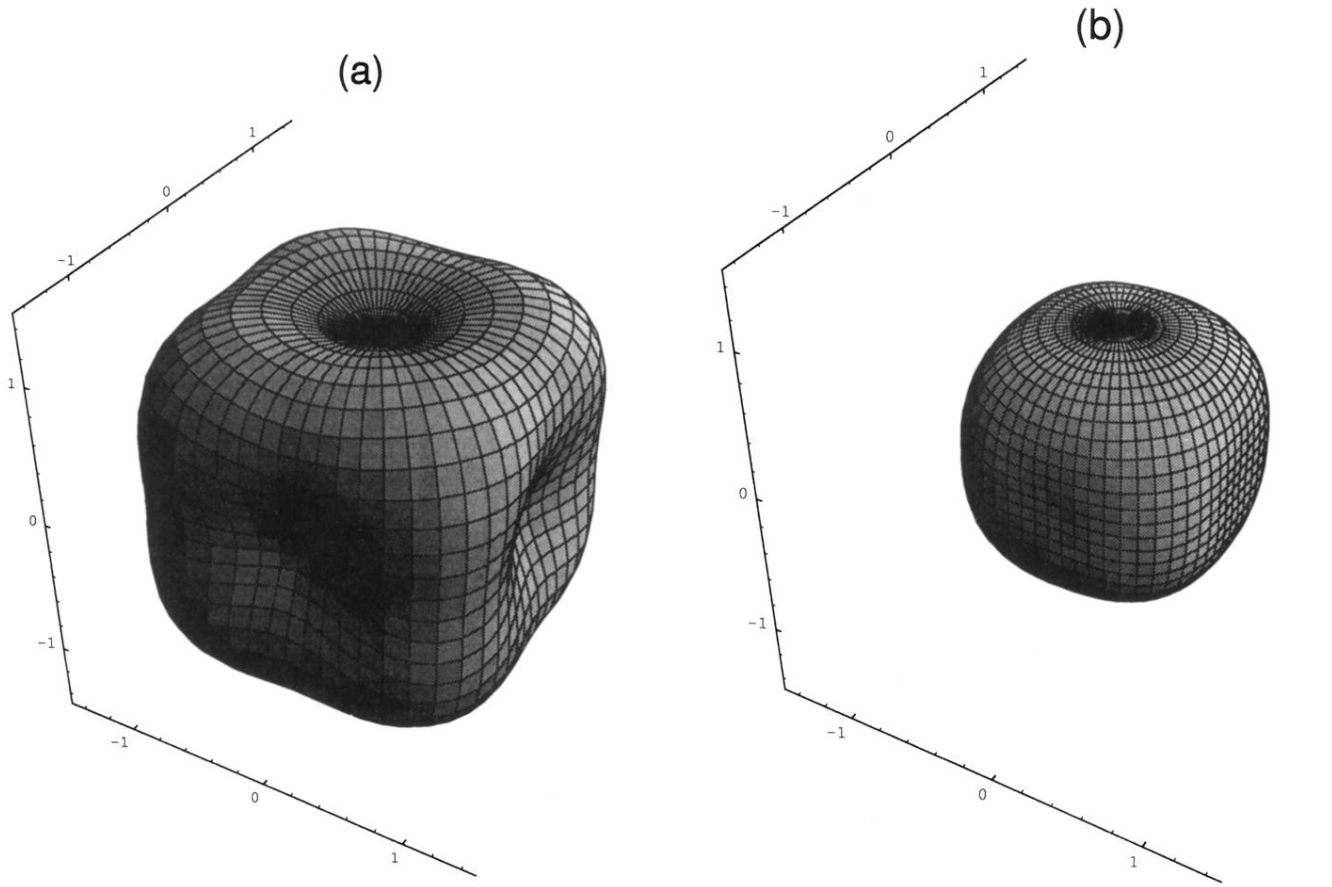

FIG. 8. The anisotropy of the two-photon-absorption coefficients of GaAs calculated from the present model: (a) For linearly polarized light, $\beta^L(\theta,\phi)/\beta^L[001]$ is plotted as a function of angle. The origin for the polarization vector $\hat{\mathbf{e}}$ is at the center of the figure. (b) For circularly polarized light, $\beta^C(\theta_\kappa,\phi_\kappa)/\beta^L[001]$ is plotted as a function of the orientation of the propagation direction $\hat{\kappa}$. The axes in the figures correspond to the crystallographic-axis directions.